Coupled-Mode Analysis of Highly Asymmetric Directional Couplers With Periodic Perturbation

B.-H. V. Borges and P. R. Herczfeld, *Fellow, IEEE*

***Abstract*— This paper presents an in-depth analysis of highly asymmetric grating assisted directional couplers. The directional coupler consists of a polymer waveguide with dimensions and refractive indices closely matching a single-mode fiber fabricated atop a $Ga_{0.6}Al_{0.4}As/GaAs/Ga_{0.4}Al_{0.6}As$ waveguide. The structure is investigated analytically by means of a new orthogonal coupled-mode theory formulated in terms of the Lorentz reciprocity theorem. For the first time, the analysis includes three distinct loss mechanisms, namely, the leakage of power toward the semiconductor substrate, the power lost to radiation modes (mode mismatching), and the grating radiation loss.**

***Index Terms*— Directional couplers, grating radiation, leaky modes, polymer, radiation modes.**

I. Introduction

COUPLING from single-mode fibers to rectangular waveguides has been the subject of investigation for many years. The reason lies in the fact that a significant amount of power is lost as these two waveguides are coupled to each other. The main loss mechanisms in fiber to rectangular waveguide coupling are the Fresnel reflections, due to the impedance mismatching at fiber/waveguide interface, and the discrepancy between the fiber (cylindrical) and waveguide (rectangular) geometry. Therefore, it is not surprising that numerous ideas have proliferated in the literature regarding structures that yield the lowest insertion loss. The most natural approach for the problem consists of utilizing waveguides with dimensions and refractive indices closely matching a single-mode fiber. This has been investigated by Hammer *et al.* [1] who utilized a polished single-mode fiber $(n \approx 1.5)$ grating coupled to a $LiNb_xTa_{1-x}O_3$ $(n \approx 2.2)$. Coupling efficiency of 6% was observed with this configuration. The low coupling efficiency is attributed to the leakage of power from the upper waveguide toward the higher refractive index substrate. Recently, Sun *et al.* [2] have investigated highly asymmetric couplers for application in wavelength-division-multiplexed (WDM) sources, consisting of a WDM laser integrated with silica glass waveguide to facilitate the coupling to a single-mode fiber. The structure was analyzed in terms of Floquet theory.

Manuscript received December 10, 1997; revised December 10, 1997. This work was supported in part by the Brazilian Research Council (RHAE) under Grant 260150/92-4.

B.-H. V. Borges was with the Center for Microwave and Lightwave Engineering, Drexel University, Philadelphia, PA, 19104 USA. He is now with the University of São Paulo, 13560-970, São Carlos, São Paulo, Brazil.

P. R. Herczfeld is with the Center for Microwave and Lightwave Engineering, Drexel University, Philadelphia, PA, 19104 USA.

Publisher Item Identifier S 0018-9480(98)02034-1.

The analysis contained in this paper considers a different approach. A polymeric waveguide, with refractive indices and thicknesses approximating a single-mode optical fiber, is fabricated atop a $Ga_{0.6}Al_{0.4}As/GaAs/Ga_{0.4}Al_{0.6}As$ asymmetric waveguide. Light from a single-mode fiber is coupled initially into the polymer waveguide and then transferred to the semiconductor guide. The phase mismatch between polymer and semiconductor modes is compensated by a diffraction grating patterned at the interface between polymer and semiconductor upper clad. The objective in this study is to provide a better understanding of the loss mechanisms involved when coupling light between two very dissimilar waveguides. The high refractive index step between polymer $(n = 1.56)$ and semiconductor guide $(n = 3.4092)$ results in a significant leakage toward the semiconductor substrate which must be considered. Since the configuration is a directional coupler, the natural approach consists of finding a coupled-mode formulation capable of handling very large refractive index steps and excessive losses, which requires an orthogonal coupled-mode formulation. Nonorthogonal approaches isolate polymer and semiconductor waveguides and, therefore, discount leakage loss.

To investigate these devices, different approaches for the energy transfer mechanism have been proposed. Lee [3] and Griffel *et al.* [4] used a nonorthogonal coupled-mode formulation based on reciprocity theorem for grating assisted directional couplers. Nonorthogonal approaches represent the modes of the compound structure as a linear combination of the modes of the individual waveguides. A very simple coupled-mode approach was presented by Chen *et al.* [5] for weakly coupled waveguides and weak perturbations. Donnelly [6], Huang [7], [8], and Hong [9] utilized a more general analysis in which cross-power terms were introduced to account for the nonorthogonality of the guided modes. Haus [10], [11] and Little [12] have adopted variational analysis to obtain coupled-mode equations accounting for cross-power terms. Although nonorthogonal approach reduces the algebra involved in the formalism, it does not provide good information about the necessary length for optimum power transfer.

A more precise coupled-mode analysis requires the solution of the entire multilayer structure resulting in waveguide modes orthogonal to each other. Huang *et al.* [13] have done a similar analysis based on local normal modes, where the interaction of the optical field with the periodic grating is described by a transfer matrix formalism defined via the mode-matching technique. Local normal modes have also been used by Weiss [14] for the analysis of asymmetric directional couplers in

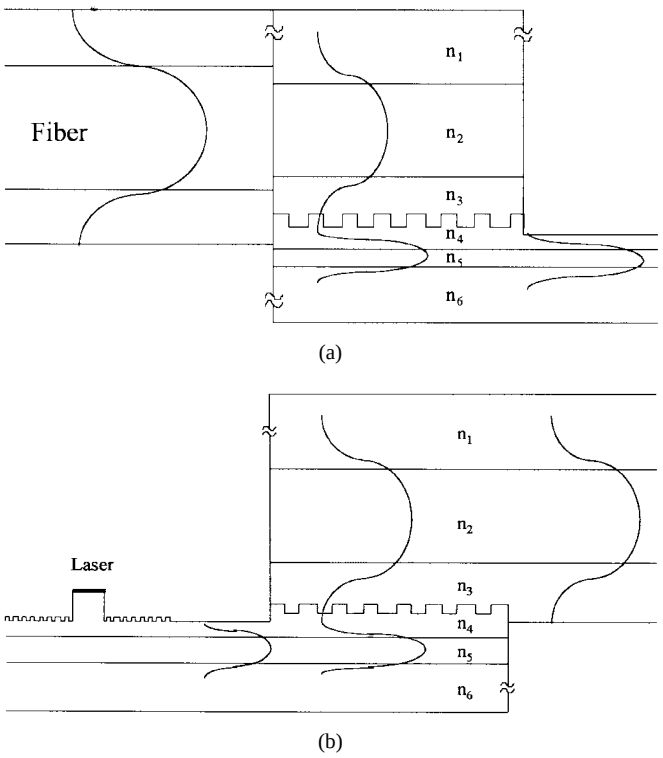

Fig. 1. Highly asymmetric directional coupler consisting of a polymer waveguide atop a semiconductor waveguide. The phase matching between polymer and semiconductor modes is provided by a diffraction grating located on the interface between polymer lower clad and semiconductor upper clad. (a) Polymer waveguide excited by a single-mode fiber. (b) Semiconductor waveguide excited by a semiconductor laser.

ion-exchanged channel waveguides. Marcuse [15], [16] has developed an orthogonal coupled-mode formulation based on expansion in terms of ideal waveguide modes. This approach produces excellent results as long as the grating perturbation is weak.

This paper introduces an extended coupled-mode approach which is formulated in terms of the Lorentz reciprocity theorem. The Lorentz reciprocity theorem is desirable since it can be applied to media with either gain or loss [4], [17]. The coupled-mode equations are described in terms of the modes of the compound structure and, therefore, are orthogonal. Three major loss mechanisms are included in the analysis for the first time. These are: 1) radiation modes; 2) leaky modes; and 3) grating radiation loss.

This paper is organized as follows. Section II describes the highly asymmetric directional coupler investigated in this paper. Sections III and IV give the theoretical background utilized in this work. Section V introduces the loss mechanisms included in the analysis. A numerical analysis is provided in Section VI. Section VII presents some concluding remarks.

II. The Proposed System

The cross section of the baseline III–V structures adopted for the simulations are depicted in Fig. 1. In Fig. 1(a), a single-mode fiber is utilized as excitation for the polymer waveguide, while in Fig. 1(b) a monolithically integrated semiconductor laser excites the semiconductor waveguide. Both consist of an asymmetric GaAlAs/GaAs single-mode waveguide epitaxially grown on an n^+-GaAs substrate. The $Ga_{0.4}Al_{0.6}As$ lower clad $(n = 3.0987)$ is sufficiently thick to isolate the optical field from the lossy substrate. The top clad is comprised of a 0.887-μm-thick $Ga_{0.6}Al_{0.4}As$ $(n = 3.1989)$ layer. The 0.32-μm-thick GaAs waveguide, sandwiched between the GaAlAs clads, consists of a 0.16 μm of p-GaAs and 0.16 μm of n-GaAs layers which form a p-n junction [18], [19]. This very thin waveguide layer with the built-in junction exploits the linear and quadratic electro-optic effects, as well as the plasma, band filling, and band shrinkage effects to yield a high figure of merit for index modulation. This structure has been successfully fabricated as an integrated optic modulator operating at a wavelength of 1.3 μm. The pertinent parameters utilized in this structure are $n_1 = 1.54$, $n_2 = 1.56$, $n_3 = 1.54$, $n_4 = 3.1989$, $n_5 = 3.4092$, and $n_6 = 3.0987$ for the refractive indices, and $t_1 = \infty$, $t_2 = 2.5\,\mu$m, $t_3 = 1.0\,\mu$m, $t_4 = 0.5\,\mu$m, $t_5 = 0.32\,\mu$m, and $t_6 = \infty$ for the thicknesses, respectively.

The polymeric waveguide atop the GaAlAs upper clad is fabricated with commercially available materials, such as Norland 61,68.[1] The fabrication process begins by dispensing a polymer onto the spinning semiconductor structure to produce a 1.0-μm-thick layer $(n = 1.54)$, and later curing it with UV light. Next, another layer of polymeric material with a refractive index of 1.56 is spin deposited atop the previous layer to form a 2.5-μm-thick layer. Finally, another layer of polymer $(n = 1.54)$ is spin dispensed onto the structure and UV cured to create the upper clad [20].

III. Orthogonal Coupled-Mode Formulation

This section is concerned with the coupled-mode formulation utilized in the analysis of the highly asymmetric coupler in Fig. 2. Two important factors need to be considered: the polymer mode distribution is strongly affected by the presence of the semiconductor and a strong leakage of power from the polymer toward the semiconductor material will occur. These effects are due to the large refractive index step between the polymer and the semiconductor and necessitate an orthogonal coupled-mode approach. The derivation will be based on the coupled-mode formulation presented in [4] and [17], specifically on the integral form of the Lorentz reciprocity theorem which can be applied to media with either gain or loss. It states that any two electromagnetic fields satisfying Maxwell's equations and associated boundary conditions obey the relation

$$\frac{\partial}{\partial z}\iint[\vec{E}^{(1)}\times\vec{H}(2)-\vec{E}^{(2)}\times\vec{H}^{(1)}]\cdot\hat{z}\,dx\,dy = i\omega\iint[\varepsilon^{(2)}(x,y,z)-\varepsilon^{(1)}(x,y,z)]\vec{E}^{(1)}\cdot\vec{E}^{(2)}\,dx\,dy. \tag{1}$$

In highly asymmetric couplers, the concept of symmetric and asymmetric modes is no longer appropriate, since these modes are preferentially located either in the upper or lower slab, respectively. A more fitting definition for these modes is quasi-top (T) and quasi-bottom (B) modes. The derivation of

[1] Norland Products, Inc., New Brunswick, NJ, USA.

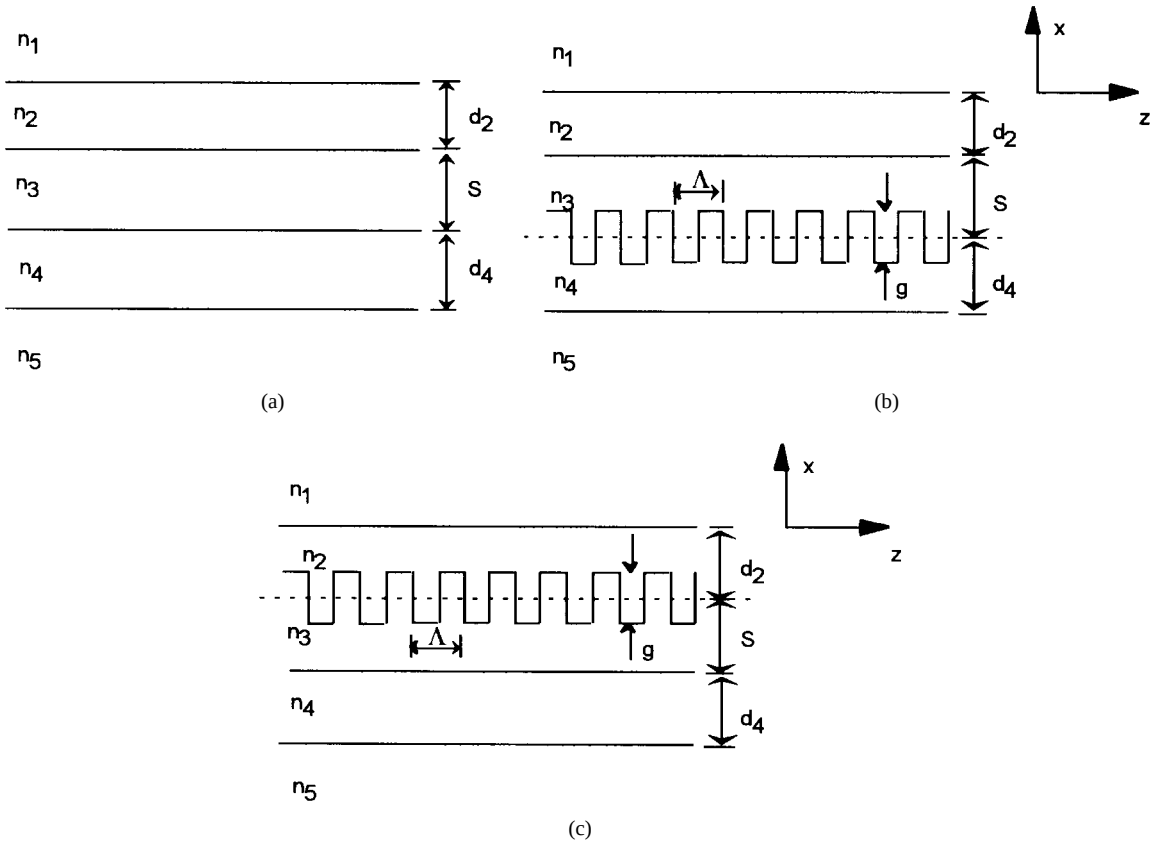

Fig. 2. Asymmetric coupled waveguide system. (a) Not phase matched. (b) and (c) Phase matched with a diffraction grating.

the coupled-mode formulation is accomplished in two steps, and for each step two sets of solutions, unperturbed and perturbed, have to be provided.

Step 1: Let the fields $\vec{E}^{(2)}$ and $\vec{H}^{(2)}$ and the permittivity $\varepsilon^{(2)}$ represent an unperturbed multilayer structure, i.e., a structure with no variation along the longitudinal direction z. Since we are concerned with asymmetric directional couplers, the energy exchange between guides is insignificant. Assume that the unperturbed mode fields can be represented by the quasi-top (T) mode solution of the multilayer waveguide

$$\varepsilon^{(2)}(x,y,z) = \varepsilon(x,y) \tag{2}$$
$$\vec{E}^{(2)}(x,y,z) = (\vec{E}_t^T - \hat{z}\vec{E}_z^T)e^{-i\beta_T z}$$
$$\vec{H}^{(2)}(x,y,z) = (-\vec{H}_t^T + \hat{z}\vec{H}_z^T)e^{-i\beta_T z}. \tag{3}$$

Now let the fields $\vec{E}^{(1)}$ and $\vec{H}^{(1)}$ and the permittivity $\varepsilon^{(1)}$ represent a perturbed multilayer structure, whose perturbation is provided by a diffraction grating. Because of the grating perturbation, the fields of the directional coupler are now able to exchange energy as they propagate along z. Therefore, the perturbed fields have to be represented by a linear combination of quasi-top **and** quasi-bottom field solutions with z-dependent amplitudes

$$\varepsilon^{(1)}(x,y,z) = \varepsilon(x,y) + \varepsilon_o \Delta n^2 f(z) \tag{4}$$
$$\vec{E}_t^{(1)}(x,y,z) = a(z)\vec{E}_t^T + b(z)\vec{E}_t^B$$
$$\vec{H}_t^{(1)}(x,y,z) = a(z)\vec{H}_t^T + b(z)\vec{H}_t^B. \tag{5}$$

The second term in (4) is the Fourier expansion of the periodic perturbation, with $f(z) = (2/\pi)\cos(2\pi z/\Lambda)$ and $\Delta n^2 = n_j^2 - n_{j-1}^2$ $(j = 2,3,\cdots,N)$. Equation (5) is the transverse component of the perturbed field. The longitudinal components are obtained via Maxwell equations as follows:

$$\vec{E}_z = -\frac{1}{\omega\varepsilon}\nabla_t \times H_t \quad \vec{H}_z = \frac{1}{i\omega\mu}\nabla_t \times E_t.$$

Therefore, the total perturbed fields become

$$\vec{E}^{(1)}(x,y,z) = a(z)\left(\vec{E}_t^T + \hat{z}\,\frac{\varepsilon^{(2)}}{\varepsilon^{(1)}}\,\vec{E}_z^T\right) + b(z)\left(\vec{E}_t^B + \hat{z}\,\frac{\varepsilon^{(2)}}{\varepsilon^{(1)}}\,\vec{E}_z^B\right) \tag{6}$$

$$\vec{H}^{(1)}(x,y,z) = a(z)(\vec{H}_t^T + \hat{z}(\vec{H}_z^T) + b(z)(\vec{H}_t^B + \hat{z}\vec{H}_z^B). \tag{7}$$

Substituting (2)–(4), (6), and (7) into (1) results (after some algebraic manipulation) in an expression for $a(z)$:

$$\frac{da(z)}{dz} = i[\beta_T + K_{TT}f(z)]a(z) + iK_{BT}f(z)b(z) \tag{8}$$

where the coupling coefficient K_{mn} $(m,n = B,T)$ is given by

$$K_{mn} = \frac{\omega\varepsilon_o\Delta n^2}{4}\iint\left[\vec{E}_t^m \cdot \vec{E}_t^n - \frac{\varepsilon^{(2)}}{\varepsilon^{(1)}}\,\vec{E}_z^m \cdot \vec{E}_z^n\right]dx\,dy, \qquad m,n = \mathrm{T,B}. \tag{9}$$

Step 2: As before, let the fields $\vec{E}^{(2)}$ and $\vec{H}^{(2)}$ and the permittivity $\varepsilon^{(2)}$ represent again an unperturbed multilayer structure, and assume the unperturbed mode fields can be represented by the quasi-bottom (B) modes

$$\varepsilon^{(2)}(x,y,z) = \varepsilon(x,y) \tag{10}$$

$$\vec{E}^{(2)}(x,y,z) = (\vec{E}_t^B - \hat{z}\vec{E}_z^B)e^{-i\beta_B z}$$

$$\vec{H}^{(2)}(x,y,z) = (-\vec{H}_t^B + \hat{z}\vec{H}_z^B)e^{-i\beta_B z}. \tag{11}$$

Assume the same perturbed solution as in Step 1

$$\varepsilon^{(1)}(x,y,z) = \varepsilon(x,y) + \varepsilon_o \Delta n^2 f(z) \tag{12}$$

$$\vec{E}^{(1)}(x,y,z) = a(z)\left(\vec{E}_t^T + \hat{z}\,\frac{\varepsilon^{(2)}}{\varepsilon^{(1)}}\,\vec{E}_z^T\right) + b(z)\left(\vec{E}_t^B + \hat{z}\,\frac{\varepsilon^{(2)}}{\varepsilon^{(1)}}\,\vec{E}_z^B\right) \tag{13}$$

$$\vec{H}^{(1)}(x,y,z) = a(z)(\vec{H}_t^T + \hat{z}\vec{H}_z^T) + b(z)(\vec{H}_t^B + \hat{z}\vec{H}_z^B). \tag{14}$$

Substituting (10)–(14) into (1) results in a first-order derivative equation for $b(z)$

$$\frac{db(z)}{dz} = iK_{TB}f(z)a(z) + i[\beta_B + K_{BB}f(z)]b(z). \tag{15}$$

The coupling coefficients K_{TB} and K_{BB} are defined as in (9). The effect of the losses can be readily visualized in (8) and (15) if one allows the propagation constants $\beta_{T,B}$ to be complex, i.e.,

$$\beta_T' = \beta_T - i\alpha_T \quad \beta_B' = \beta_B - i\alpha_B \tag{16}$$

where the α's represent propagation losses. Before substituting (16) in the coupled equations (8) and (15), one must realize that the field amplitudes $a(z)$ and $b(z)$ are rapid varying functions of z. These rapid oscillations can be eliminated by introducing slowly varying amplitudes, such that

$$a(z) = A(z)e^{i(\beta_T + i\alpha_T)z} \quad b(z) = B(z)e^{i(\beta_B + i\alpha_B)z}. \tag{17}$$

Substituting (16) and (17) into (8) and (15) results in the following:

$$\frac{dA(z)}{dz} = i[K_{TT}f(z) - i2\alpha_T]A(z) + iK_{BT}f(z) \cdot e^{i(\beta_B - \beta_T)z}e^{(\alpha_T - \alpha_B)z}B(z) \tag{18}$$

$$\frac{dB(z)}{dz} = iK_{TB}f(z)e^{i(\beta_T - \beta_B)z}e^{(\alpha_B - \alpha_T)z}A(z) + i[K_{BB}f(z) - i2\alpha_B]B(z). \tag{19}$$

Equations (18) and (19) are the coupled-mode equations employed in the analysis of the highly asymmetric coupler in Fig. 1.

IV. Power Conservation for Lossless Structure

In a lossless structure (the transverse components of the electric and magnetic fields and respective longitudinal propagation constants are real quantities), the coupling coefficients K_{mn} $(m,n = T,B)$ are also real, and the optical power associated with the fields is

$$P(z) = \tfrac{1}{2}\mathcal{R}\left(\iint [|a(z)|^2\vec{E}_t^T \times \vec{H}_t^{T^*} + a(z)b^*(z)\vec{E}_t^T \times \vec{H}_t^{B^*} + a^*(z)b(z)\vec{E}_t^B \times \vec{H}_t^{T^*} + |b(z)|^2\vec{E}_t^B \times \vec{H}_t^{B^*}]\right) \cdot \hat{z}\,dx\,dy \tag{20}$$

where we used (5). Equation (20) can be simplified with the help of the overlapping integral

$$C_{mn} = \tfrac{1}{2}\iint \vec{E}_t^n \times \vec{H}_t^m \cdot \hat{z}\,dx\,dy, \qquad m,n = \mathrm{T,B} \tag{21}$$

where $C_{TT} = C_{BB} = 1$ and $C_{TB} = C_{BT} = 0$. Expanding (20) and making use of (21) results in the following:

$$P(z) = |a(z)|^2 + |b(z)|^2.$$

Power conservation requires $(d/dz)P(z) = 0$, which results in the following:

$$K_{BT} - K_{TB}^* = 0. \tag{22}$$

Equation (22) is completely satisfied by this orthogonal coupled-mode formulation.

V. Loss Mechanisms

The analytical tools necessary to calculate the individual loss terms are developed next. Three important loss mechanisms are considered in this section, namely, leakage loss, radiation modes, and grating radiation loss.

A Leakage Loss

A waveguide fabricated with low refractive index materials (such as polymer) fabricated atop a high index material (such as semiconductor) acts as a leaky guide. This leakage of power toward the higher index material results in attenuation represented by a complex propagation constant. More specifically, the rate of power leaked is identified by the imaginary part of the propagation constant which can be obtained via a transfer matrix method, summarized here for completeness. A full derivation can be found in [21].

Considering a general multilayered planar waveguide system, the solution of the Helmholtz wave equation in each layer j is given by

$$E_j(x) = A_j e^{\gamma_j(x - t_j)} + B_j e^{-\gamma_j(x - t_j)} \quad \text{with}$$

$$\gamma_j = \sqrt{\beta^2 - k_0^2 n_j^2}, \qquad j = 1,2,3,\cdots,N.$$

Since only TE modes are considered in this analysis, the following boundary conditions must be satisfied at each interface as follows:

$$E_j(t_j) = E_{j-1}(t_j)$$

$$\frac{\partial}{\partial x}E_j(t_j) = \frac{\partial}{\partial x}E_{j-1}(t_j), \qquad j = 1,2,\cdots,N-1.$$

The transfer matrix is then obtained by recursively matching the electric field and its derivatives at each interface and combining the resulting equations into a matrix form:

$$\begin{bmatrix} A_1 \\ B_1 \end{bmatrix} = T_{wg} \begin{bmatrix} A_N \\ B_N \end{bmatrix}$$

where

$$T_{wg} = \prod_{j=2}^{N} T_j = \begin{bmatrix} t_{11} & t_{12} \\ t_{21} & t_{22} \end{bmatrix}$$

$$T_j = \begin{bmatrix} \frac{1}{2}\left(1+\frac{\gamma_j}{\gamma_{j-1}}\right)e^{-\theta_j} & \frac{1}{2}\left(1-\frac{\gamma_j}{\gamma_{j-1}}\right)e^{\theta_j} \\ \frac{1}{2}\left(1-\frac{\gamma_j}{\gamma_{j-1}}\right)e^{-\theta_j} & \frac{1}{2}\left(1+\frac{\gamma_j}{\gamma_{j-1}}\right)e^{\theta_j} \end{bmatrix}$$

$$\theta_j = \gamma_j(t_j - t_{j-1}) = 2_j\gamma_j.$$

The leakage is then calculated by solving for $t_{21}(\beta) = 0$ via the "downhill method" [22] for the complex propagation constants.

B. Radiation Modes

Radiation modes constitute a continuum of modes which are not confined in the core. They are excited at the input of the waveguide due to mode mismatch of the polymer guide and the butt coupled fiber and due to geometrical imperfections [16]. The study of these modes is complicated by the fact that a infinitely number can be excited. This problem can be greatly simplified if the waveguide structure is assumed to be bounded by metallic walls located very far away from the guiding structure. This artifice transforms the continuous spectrum of radiation modes into a discrete and orthogonal set of modes [23].

Assuming that all guided and radiation modes can be obtained with this technique, these modes can then be connoted by $E_i(x)$, where $i = 1, 2, 3, \cdots$, extends over guided and radiation modes. If $E_i(x)$ represents a complete set of orthogonal modes, then it constitutes a basis and, therefore, the field of the optical fiber can be written as

$$\psi(x) = \sum_i c_i E_i(x) \tag{23}$$

where the c_i's are expansion coefficients. To obtain the power distribution in all modes (guided and radiation) inside the rectangular structure, the expansion coefficients must be determined. To do so, multiply (23) by $E_j^*(x)$ and integrate

$$(E_j(x), \psi(x)) = \left(E_j(x), \sum_i c_i E_i(x)\right) \tag{24}$$

where $(E_j, \psi) = \int E_j^* \psi \, dx$.

The right-hand side (RHS) of (24) may be expanded:

$$\left(E_j, \sum_i c_i E_i\right) = c_1(E_j, E_1) + c_2(E_j, E_2) + \cdots + c_j(E_j, E_j) + \cdots + c_n(E_j, E_n) + \cdots. \tag{25}$$

Using the orthogonality of the fields in (25), we obtain

$$\left(E_j, \sum_i c_i E_i\right) = c_j. \tag{26}$$

Substituting (26) into the RHS of (24) gives

$$(E_j(r), \psi(r)) = c_j \quad \text{or} \quad c_i = \int E_i^*(x)\, \psi(x)\, dx. \tag{27}$$

Equation (27) represents the overlap between the guided or radiation modes inside the waveguide and the fiber mode, and it is considered as a measure of energy lost to radiation modes at the input of the coupler.

C. Grating Radiation

This section accounts for the radiation properties of gratings in asymmetric directional couplers. The analysis is an extension of the study on grating radiation in GaAs:GaAlAs lasers by Streifer [24] to multilayer directional couplers. The wave equation for a longitudinally varying structure can be written as

$$\left[\frac{d^2}{dx^2} + (k_0^2 n_0^2 - \beta_n^2)\right] E_n(x) = -k_0^2 \sum_{m=-\infty}^{\infty} E_m(x) A_{n-m} \tag{28}$$

where $A_q = (n_5^2 - n_3^2/q\pi)\sin(q(\pi/2)), \beta_n = \beta_0 + 2\pi n/\nabla$, and ∇ is the grating period. The Fourier coefficient A_q is different from zero inside the grating region and for $q \neq 0$, and equal to zero outside. n_0 is the average refractive index of the grating which is given by $n_0^2 = n_3^2 + n_5^2/2$. Equation (28) can be further simplified if one assumes that all partial waves $E_n(x)$ are driven by the fundamental wave $E_0(x)$, which results in a first-order perturbation equation for $E_n(x)$:

$$\left[\frac{d^2}{dx^2} + (k_0^2 n_0^2 - \beta_n^2)\right] E_n(x) = -k_0^2 E_0(x) A_n. \tag{29}$$

The RHS of (29) is equal to zero outside the grating layer and also for $q = 0$, which allows us to write the solution in terms of homogeneous ordinary differential equations. This is no longer true in the grating region since the RHS becomes different from zero ($q \neq 0$). Since the grating layer is assumed homogeneous, the six-layer structure is now converted into a seven-layer structure, as shown in Fig. 3. The thickness of the new layer is given by the grating height and the refractive index by the average index n_0. For $n = 0$, the RHS of (29) is zero, so β_0 is calculated by solving $\det(\boldsymbol{Q}) = 0$, as shown in the Appendix. Once β_0 is calculated β_n ($-\infty \leq n \leq \infty, n \neq 0$) is obtained according to

$$\beta_n = \beta_0 + n\,\frac{2\pi}{\Lambda}, \qquad n = 0, \pm 1, \pm 2, \pm 3, \cdots$$

where Λ is the grating period. The power lost by each partial wave $E_n(x)$ is calculated via a Poynting vector, which gives

$$P_n = \frac{1}{2\omega\mu_0}\, \mathcal{R}\{\sqrt{k_0^2 n_1^2 - \beta_n^2}|E_n(-t_2 - t_3)|^2 + \sqrt{k_0^2 n_7^2 - \beta_n^2}|E_n(t_4 + t_5 + t_6)|^2\}$$

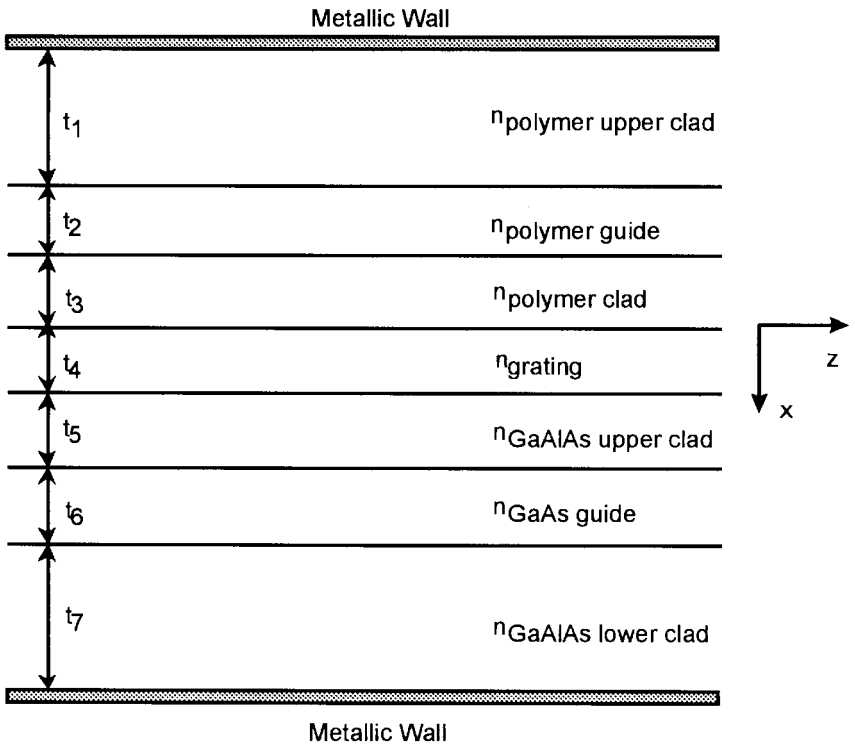

Fig. 3. Longitudinal cross section of the asymmetric coupler. The diffraction grating is substituted by an homogeneous layer with refractive index $n_0^2 = n_3^2 + n_5^2/2$ and thickness equal to the grating height.

where the first term corresponds to the radiated power into region 1, and the second term to the radiated power into region 7. Finally, the expression for the total radiated power by the grating is given by [24]

$$\alpha = \sum_{n=-\infty}^{\infty} P_n$$

with P_n normalized in terms of the power of the fundamental mode $(n = 0)$. Now that all the loss mechanisms are described, we can study the performance of the coupler as a function of its pertinent parameters.

VI. Numerical Examples

To validate the theory elaborated in this paper, we utilize the examples indicated in [15] for TE and TM polarizations. The longitudinal cross section of the directional coupler is shown in Fig. 2(b) and (c), and the pertinent values for the refractive indices and thicknesses of the layers are $n_1 = 3.20$, $n_2 = 3.25$, $n_3 = 3.20$, $n_4 = 3.23$, and $n_5 = 3.20$, $d_2 = 1.0\,\mu$m, and $d_4 = 1.0\,\mu$m. The grating depth for all examples is 0.1 μm and the wavelength $\lambda = 1.5\,\mu$m. A critical parameter in grating assisted directional couplers is the grating periodicity Λ. As in [15], the grating periodicity $\Lambda = 2\pi/(\beta_T - \beta_B)$.

Consider initially, TE polarization [$E_z = 0$ in (21)]. Having calculated the electric- and magnetic-field distributions for the compound waveguide structure, we are now able to solve the coupled-mode equations (18) and (19). This system of ordinary differential equation is integrated using fourth- and fifth-order Runge–Kutta formulas [23]. The initial conditions at $z = 0$ μm are $A(0) = A_0$ and $B(0) = 0$. Two different grating locations are also considered in this example: grating on the interface n_3 and n_4 [Fig. 2(b)] $\Delta n^2 = n_4^2 - n_3^2$, and grating on the interface n_2 and n_3 [Fig. 2(c)] $\Delta n^2 = n_2^2 - n_3^2$. The coupling length L_π for total transfer of energy as a function of the waveguide separation S is shown in Fig. 4. The results obtained with TM polarization for this structure is shown in Fig. 5. The agreement with the ideal mode expansion observed for both polarizations is once again remarkable. The discontinuity observed near $S \approx 1.1$ μm (TE) and $S \approx 0.9$ μm (TM) is due to a zero crossing of the mode field distribution of the asymmetric mode inside the grating region. This causes the coupling coefficient in (21) to vanish, resulting in an infinite coupling length [15]. This behavior is not observed in nonorthogonal coupled-mode formulations, once the structure is analyzed in terms of the modes of isolated waveguides.

The extended coupled-mode analysis is now applied to the highly asymmetric structures depicted in Fig. 1. The objective is to gain some insight on how the thicknesses of the different layers of these asymmetric structures as well as the grating depth act upon the loss mechanisms. Two different excitation conditions are considered: a single-mode fiber butt coupled to the polymer waveguide [Fig. 1(a)], and of a semiconductor laser monolithicaly integrated with the semiconductor waveguide [Fig. 1(b)]. The wavelength used in both cases is 1.3 μm.

A. Excitation From a Single-Mode Fiber

1) Influence of the Polymer Clad Thickness, t_3: In this simulation the polymer lower clad thickness t_3 is allowed to vary from 0 to 3.0 μm, while the GaAlAs upper clad

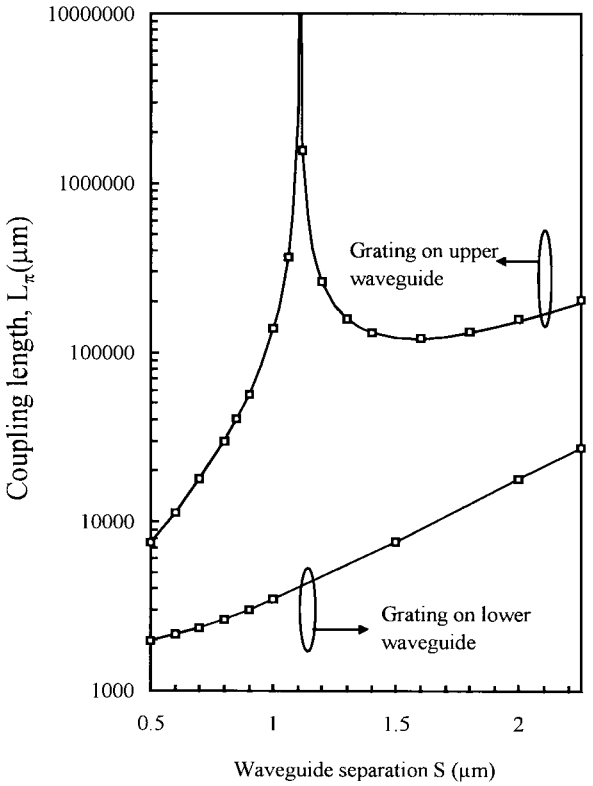

Fig. 4. Coupling length as a function of the waveguide separation for a directional coupler close to synchronism. Solid line is obtained with the ideal mode expansion [15], and squares with the present theory.

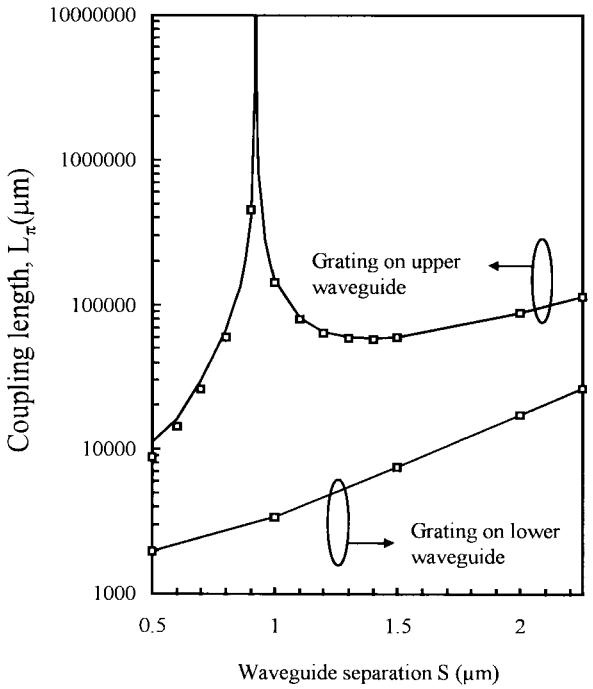

Fig. 5. Coupling length as a function of the waveguide separation for a directional coupler close to synchronism for TM polarization. Solid line is obtained with the ideal mode expansion [15], and squares with the present theory.

thickness t_4 is held at 0.5 μm. Leakage loss, as expected, decreases with the increase of t_3 by virtue of the smaller penetration of the exponential tail of the polymer mode into

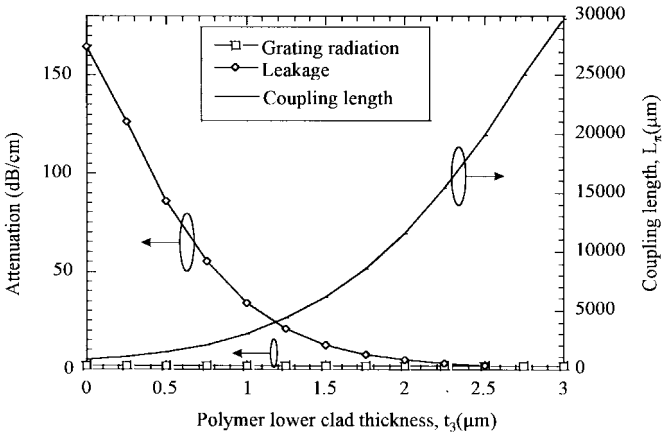

Fig. 6. Leakage (diamonds), grating radiation loss (squares), and coupling length (solid line) versus polymer lower clad thickness t_3.

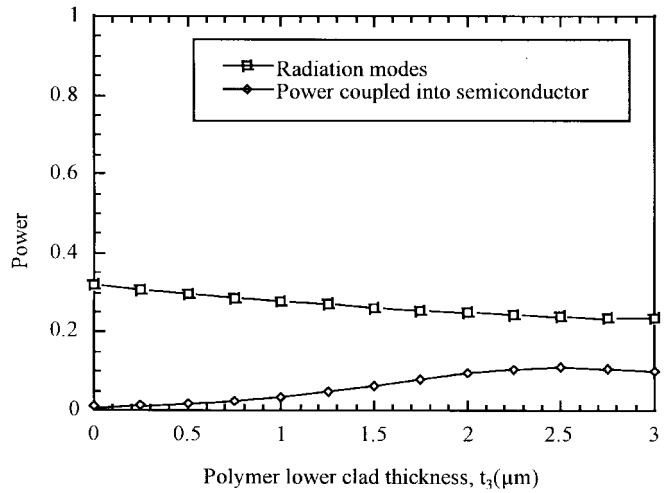

Fig. 7. Power transfer efficiency versus polymer lower clad thickness t_3. The power coupled into the semiconductor guide is shown as diamonds, and the power lost to radiation modes as squares.

the semiconductor, as shown in Fig. 6 (diamonds). The grating radiation loss (squares) and the coupling length (solid line) as a function of t_3 are also shown in this figure. The propagation constants in the polymer and semiconductor waveguides are barely affected by changes in t_3, thus the grating attenuation loss, on the other hand, remains reasonably constant. As the thickness of the polymer lower clad increases, a better overlap between fiber and polymer modes is attained, resulting in lower radiation mode losses (squares), as seen in Fig. 7. The total losses are too large to allow any significant transfer of power from the polymer to the semiconductor guide. The maximum power transfer is 11% for $t_3 = 2.5$ μm with a coupling length $L_\pi = 19936$ μm.

2) Influence of the GaAlAs Upper Clad Thickness t_4: The range of variation for t_4 (from 0.5 to 1.0 μm) was chosen in such a way that the semiconductor waveguide still remains single mode. The substrate leakage loss (squares), the grating radiation loss (diamonds), and the device coupling length (solid line) are shown in Fig. 8. Simulations of the coupled-mode solution are plotted in Fig. 9. The power lost to radiation modes (squares), as expected, is independent of

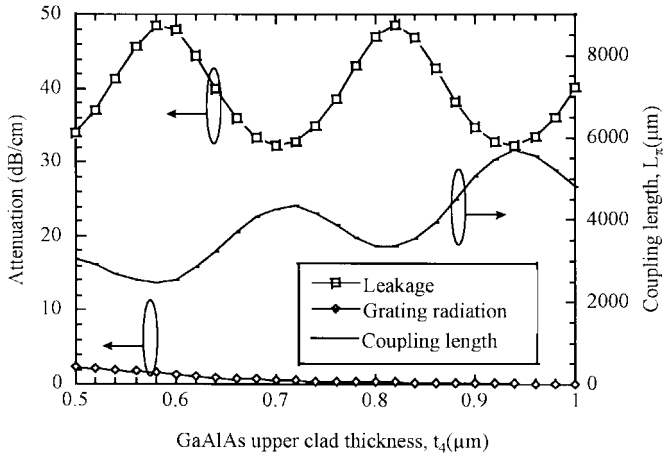

Fig. 8. Leakage (squares) and grating radiation loss (diamonds) versus GaAlAs upper clad thickness t_4.

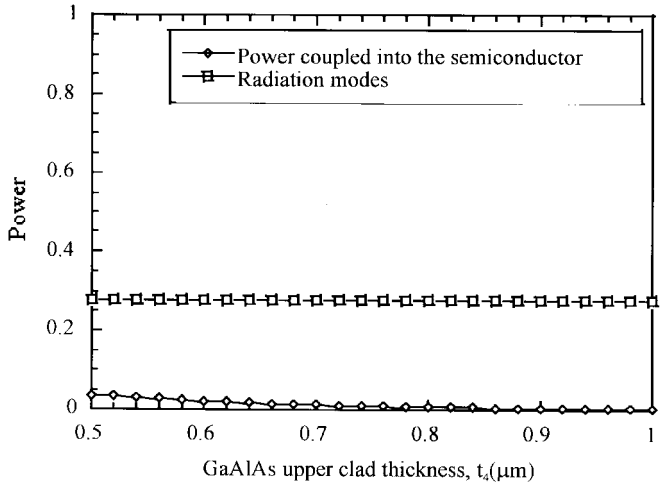

Fig. 9. Power transfer efficiency versus GaAlAs upper clad thickness t_4. The power coupled into the semiconductor guide is shown as diamonds, and the power lost to radiation modes as squares.

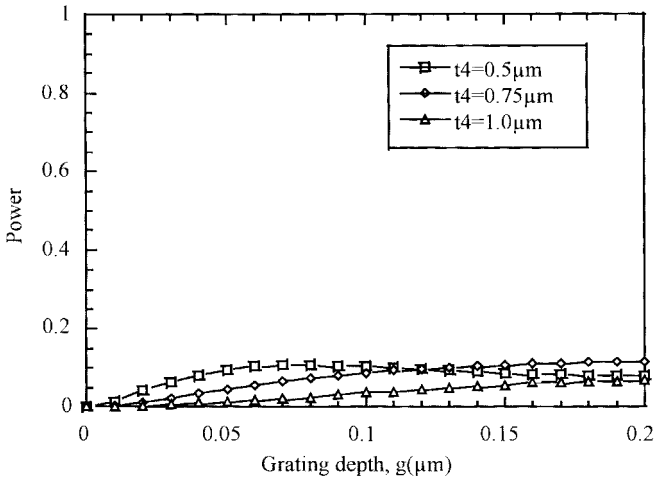

Fig. 10. Coupled power into semiconductor waveguide versus grating depth g with GaAlAs upper clad thickness t_4 as a parameter. Polymer lower clad $t_3 = 1.5$ μm.

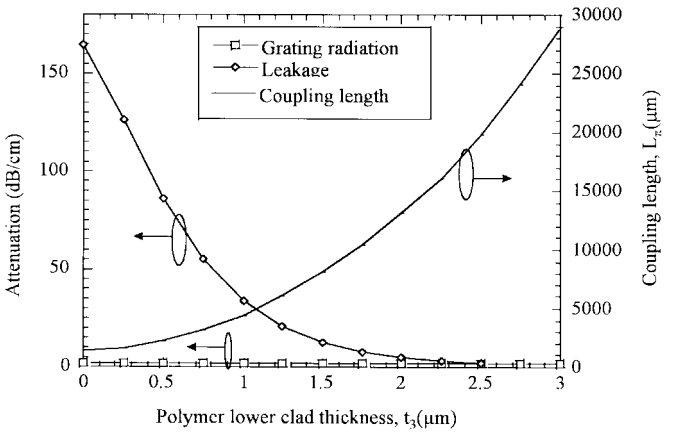

Fig. 11. Leakage (diamonds), grating radiation loss (squares), and coupling length (solid line) versus polymer lower clad thickness t_3.

the semiconductor upper clad thickness. The maximum power transfer is a mere 3.5% for $t_4 = 0.5$ μm. The decrease of the coupled power with increase of t_4 is due to the fast exponential decay of the semiconductor field in the grating region.

3) Influence of the Grating Depth g: In all the preceding examples, the grating depth was fixed at 300 Å. To investigate the influence of this parameter on the power transfer efficiency of the coupler, the grating depth is allowed to vary from 0 to 3000 Å. The polymer lower clad thickness t_3 is fixed on 1.5 μm. The GaAlAs clad thickness $t_4 = 0.5$, 0.75, and 1.0 μm is utilized as a parameter in this simulation. The power transfer efficiency from polymer to semiconductor waveguide is now calculated by solving the coupled-mode equations (18) and (19). The coupled power as a function of grating depth for $t_3 = 1.5$ μm and t_4 as a parameter is shown in Fig. 10. The best coupling condition (10.7%) is achieved for $t_4 = 0.5$ μm and $g = 0.08$ μm with $L_\pi = 2869.7$ μm. In this example, the power coupled into the semiconductor reaches a saturation point and then starts falling again as a consequence of the losses. The calculations show that further reduction in the GaAlAs upper clad thickness t_4 cuts the semiconductor mode off. Therefore, no improvement in the coupling efficiency from polymer to semiconductor waveguide can be achieved.

B. Excitation from an Integrated Semiconductor Laser

1) Influence of the Polymer Clad Thickness t_3: As in Section VI-A, the polymer lower clad t_3 is varied again from 0 to 3.0 μm while the GaAlAs upper clad t_4 is held at 0.5 μm. Leakage, grating radiation, and coupling length are shown as function of the polymer thickness t_3 in Fig. 11. Leakage and grating radiation losses are calculated independently of the type of excitation and, therefore, are the same as in Section VI-A. The solution of the coupled-mode equations for this example is given in Fig. 12 with squares representing the power lost to radiation modes, and diamonds the power transferred to the polymer waveguide. Since the semiconductor waveguide is an extension of the semiconductor laser used as excitation, the laser and waveguide modes overlap to ~1, drastically reducing the radiation mode loss. This figure shows an opposite tendency for the coupled power if compared to the example depicted in Fig. 7, which is caused

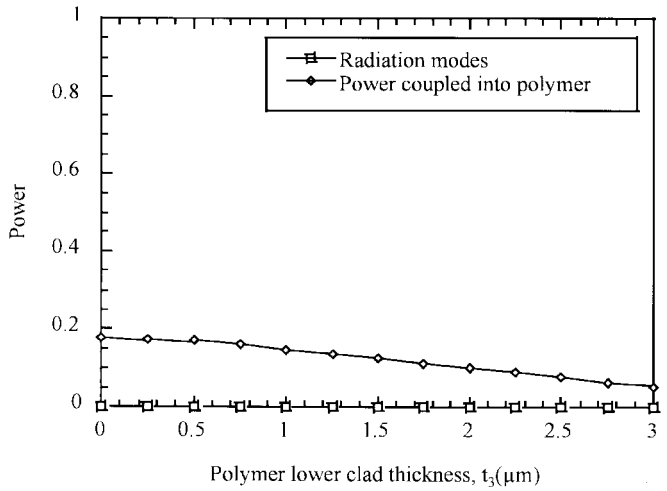

Fig. 12. Power transfer efficiency versus polymer lower clad thickness t_3. The power coupled into the polymer guide is shown as diamonds, and the power lost to radiation modes as squares.

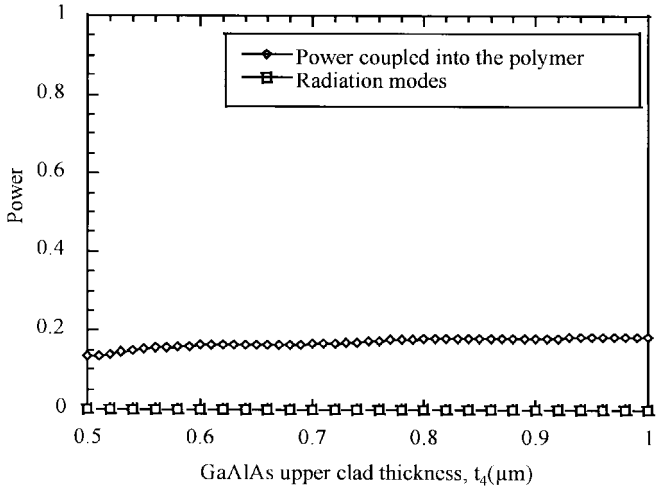

Fig. 14. Power transfer efficiency as a function of the GaAlAs upper clad thickness t_4. The power coupled into the polymer guide is shown as diamonds, and the power lost to radiation modes as squares.

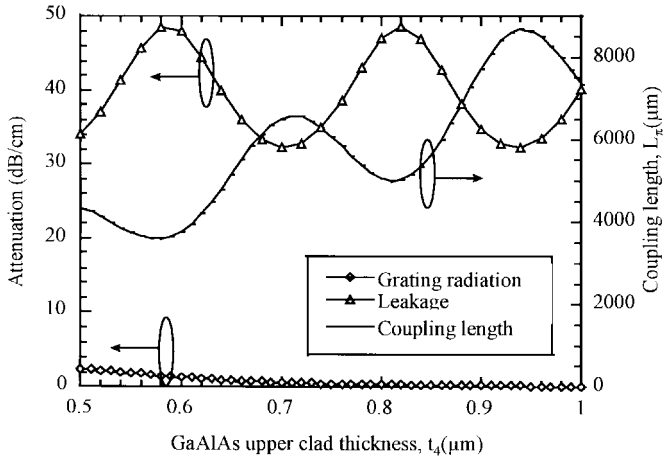

Fig. 13. Leakage (triangles) and grating radiation loss (diamonds) versus GaAlAs upper clad thickness t_4.

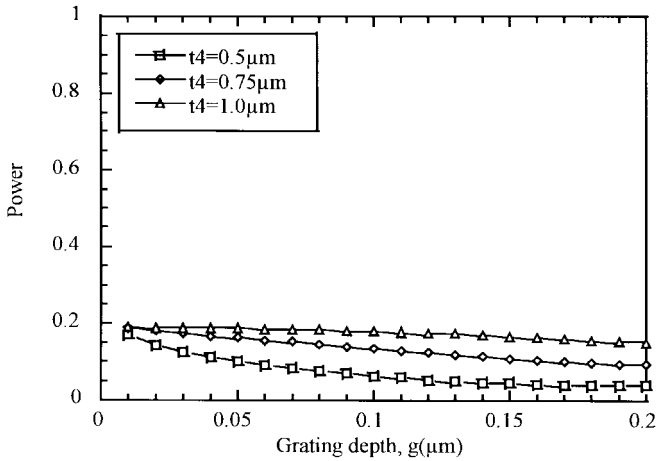

Fig. 15. Coupled power into polymer waveguide versus grating depth g with GaAlAs upper clad thickness t_4 as a parameter. Polymer lower clad $t_3 = 1.5$ μm.

by the insignificant radiation mode loss (squares) and by the extremely low loss experienced by the semiconductor mode. Consequently, the polymer guide has more energy available to receive, resulting in better coupling efficiency.

2) Influence of the GaAlAs Upper Clad Thickness t_4: As in Section VI-A, the thickness of the GaAlAs upper clad t_4 is allowed to vary from 0.5 to 1.0 μm while the thickness of the polymer lower clad t_3 is fixed at 1.0 μm. Leakage (triangles), grating radiation (diamonds), and coupling length (solid line) as a function of t_4 are shown in Fig. 13. A discussion about these quantities is provided in Section VI-A. The coupled-mode solution for this example is given in Fig. 14, with squares representing the power lost to radiation modes, and diamonds the power transferred to the polymer waveguide. The subtle increase of the coupled power, observed as t_4 increases, suggesting that less energy is lost along the longitudinal direction when the semiconductor mode field confinement is increased. As a result, the energy stays longer in the semiconductor waveguide before it transfers abruptly to the polymer waveguide. Since the semiconductor guide does not experience leakage loss, more energy becomes available to be transferred to the polymer waveguide. The maximum power transfer efficiency for this configuration is 18.6% for $t_4 = 0.98$ μm with a corresponding coupling length L_π of 7284.6 μm.

3) Influence of the Grating Depth g: In this section, the grating depth is allowed to vary from 0 to 3000 Å. Again, the thickness of the polymer lower clad t_3 is held at 1.5 μm while the thickness of the GaAlAs takes three different values $t_4 = 0.5$, 0.75, and 1.0 μm. Coupled power as a function of grating depth g for $t_3 = 1.5$ μm and t_4 as a parameter is shown in Fig. 15. The coupled power shows an opposite tendency if compared to the results obtained in Section VI-A, i.e., more coupling is obtained for shallower gratings and thicker GaAlAs upper claddings. The best coupling efficiencies for the structure investigated in this section was obtained for $t_4 = 1.0$ μm and $g = 100$ Å and is 19%. The simulations show that the maximum coupling efficiency from semiconductor to polymer guide is limited by the thickness of the polymer lower clad t_3.

VII. Conclusions

This paper presented an in-depth analysis of the performance of highly asymmetric directional couplers. A new approach for describing the energy transfer mechanism in a grating assisted directional coupler has been formulated. This approach was derived aimed at the investigation of highly asymmetric directional couplers, and was formulated in terms of the integral form of the Lorentz reciprocity theorem. The numerical results agree remarkably well with the ideal mode expansion technique [15]. The resulting orthogonal technique is simple, robust, and very easy to implement. It can also be extended to complex refractive index media and strongly coupled structures. The theory was then applied to a highly asymmetric structure consisting of a polymeric waveguide fabricated on top of a semiconductor waveguide. Three different loss mechanisms were included in the analysis, namely, the leakage of power toward the semiconductor substrate, the power lost to radiation modes (mode mismatching), and the grating radiation loss. On the basis of this asymmetric structure, the following two distinct excitation conditions were investigated: a single-mode fiber butt coupled to the polymer waveguide (the results obtained for this structure predict a maximum coupling efficiency around 11%), and a laser monolithically integrated with the semiconductor waveguide. A great advantage of this configuration over the previous one consists of the drastic reduction in the loss to radiation modes, with a significant effect on the coupling efficiency to the polymer waveguide. The simulations predicted a maximum coupling efficiency of about 19% for very shallow gratings, $g \approx 100$ Å. This analysis will also be extended to other grating shapes, such as blazed gratings, which have been suggested for air-to-waveguide grating assisted coupling with very promising results.

Appendix

This appendix describes the propagation characteristics of a planar waveguide coupler with periodic perturbations. The calculation is performed via first-order perturbation analysis which assumes that all partial waves $E_n(x)$ generated by the grating are driven by the fundamental wave $E_0(x)$:

$$\left[\frac{d^2}{dx^2} + (k_0^2 n_0^2 - \beta_n^2)\right] E_n(x) = -k_0^2 E_0(x) A_n. \qquad \text{(A-1)}$$

The RHS of (A-1) is equal to zero outside the grating layer and also for $q = 0$, which allows us to write the solution in terms of homogeneous ordinary differential equations. This is no longer true in the grating region since the RHS becomes different from zero ($q \neq 0$). Since the grating layer is assumed as a homogeneous layer in this analysis, the six-layer structure is now converted into a seven-layer structure, which is assumed in this derivation as bounded by metallic walls. The thickness of the new layer is given by the grating height and the refractive index by $n_0^2 = n_3^2 + n_5^2/2$ (Fig. 3). The solution of the seven-layer structure is then written as

$$\begin{aligned}
E_{n1} &= A_{n1}\sin[k_{n1}(x+t_1+t_2+t_3)], \\
&\qquad -(t_1+t_2+t_3) \le x \le -(t_2+t_3) \\
E_{n2} &= A_{n2}\exp[ik_{n2}(x+t_3)] + B_{n2}\exp[-ik_{n2}(x+t_3)], \\
&\qquad -(t_2+t_3) \le x \le -t_3 \\
E_{n3} &= A_{n3}\exp[ik_{n3}x] + B_{n3}\exp[-ik_{n3}x], \qquad -t_3 \le x \le 0 \\
E_{n4} &= a_{n4}\exp[ik_{n4}x] + B_{n4}\exp[-ik_{n4}x] + T_n(x), \\
&\qquad 0 \le x \le t_4 \\
E_{n5} &= A_{n5}\exp[ik_{n5}(x-t_4)] + B_{n5}\exp[-ik_{n5}(x-t_4)], \\
&\qquad t_4 \le x \le t_4 + t_5 \\
E_{n6} &= A_{n6}\exp[ik_{n6}(x-t_4-t_5)] + B_{n6}\exp[-ik_{n6}(x-t_4-t_5)], \\
&\qquad t_r + t_5 \le x \le t_4 + t_5 + t_6 \\
E_{n7} &= A_{n7}\sin[k_{n7}(x-t_4-t_5-t_6-t_7)], \\
&\qquad t_4+t_5+t_6 \le x \le t_4+t_5+t_6+t_7.
\end{aligned}$$

The equation for E_{n4} corresponds to the nonhomogeneous solution, with $T_n(x)$ given by [25]

$$\begin{aligned}
T_n(x) = &-k_0^2 \frac{(n_5^2 - n_3^2)}{\pi n k_{n4}} \sin\left(n\frac{\pi}{2}\right) \\
&\cdot \int_0^x [A_{04}\exp(ik_{04}y) + B_{04}\exp(-ik_{04}y)] \\
&\cdot \sin[k_{n4}(x-y)]\, dy. \qquad \text{(A-2)}
\end{aligned}$$

The solution then continues by matching the field and its derivatives at each interface, resulting in a determinant equation for β_n such that $\boldsymbol{Q}\cdot\boldsymbol{C} = \boldsymbol{T}$, where $\boldsymbol{Q}$ is a 12×12 matrix with the coefficients multiplying each amplitude A_n and B_n, $\boldsymbol{C}$ is a column vector containing the amplitude coefficients A_{n1} and B_{n1} through A_{n7} and B_{n7}, and $\boldsymbol{T}$ is a column vector

$$\begin{bmatrix}
a_{11} & a_{12} & a_{13} & 0 & 0 & 0 & 0 & 0 & 0 & 0 & 0 & 0 \\
a_{21} & a_{22} & a_{23} & 0 & 0 & 0 & 0 & 0 & 0 & 0 & 0 & 0 \\
0 & a_{32} & a_{33} & a_{34} & a_{35} & 0 & 0 & 0 & 0 & 0 & 0 & 0 \\
0 & a_{42} & a_{43} & a_{44} & a_{45} & 0 & 0 & 0 & 0 & 0 & 0 & 0 \\
0 & 0 & 0 & a_{54} & a_{55} & a_{56} & a_{57} & 0 & 0 & 0 & 0 & 0 \\
0 & 0 & 0 & a_{64} & a_{65} & a_{66} & a_{67} & 0 & 0 & 0 & 0 & 0 \\
0 & 0 & 0 & 0 & 0 & a_{76} & a_{77} & a_{78} & a_{79} & 0 & 0 & 0 \\
0 & 0 & 0 & 0 & 0 & a_{86} & a_{87} & a_{88} & a_{89} & 0 & 0 & 0 \\
0 & 0 & 0 & 0 & 0 & 0 & 0 & a_{98} & a_{99} & a_{910} & a_{911} & 0 \\
0 & 0 & 0 & 0 & 0 & 0 & 0 & a_{108} & a_{109} & a_{1010} & a_{1011} & 0 \\
0 & 0 & 0 & 0 & 0 & 0 & 0 & 0 & 0 & a_{1110} & a_{1111} & a_{1112} \\
0 & 0 & 0 & 0 & 0 & 0 & 0 & 0 & 0 & a_{1210} & a_{1211} & a_{1212}
\end{bmatrix}
\begin{bmatrix} a_{n1} \\ A_{n2} \\ B_{n2} \\ A_{n3} \\ B_{n3} \\ A_{n4} \\ B_{n4} \\ A_{n5} \\ B_{n5} \\ A_{n6} \\ B_{n6} \\ A_{n7} \end{bmatrix}
= \begin{bmatrix} 0 \\ 0 \\ 0 \\ 0 \\ 0 \\ 0 \\ b_{71} \\ b_{81} \\ 0 \\ 0 \\ 0 \\ 0 \end{bmatrix} \qquad \text{(A-3)}$$

containing the nonhomogeneous coefficients due to the grating, shown in (A-3), at the bottom of the previous page, where

$$
\begin{aligned}
a_{11} &= \sin(k_{n1}t_1)\\
a_{12} &= -\exp(-ik_{n2}t_2)\\
a_{13} &= -\exp(ik_{n2}t_2)\\
a_{21} &= -i\frac{k_{n1}}{k_{n2}}\cos(k_{n1}t_1)\\
a_{22} &= -\exp(-ik_{n2}t_2)\\
a_{23} &= \exp(ik_{n2}t_2)\\
a_{32} &= 1, \quad a_{33} = 1\\
a_{34} &= -\exp(-ik_{n3}t_3)\\
a_{35} &= -\exp(ik_{n3}t_3)\\
a_{42} &= 1\\
a_{43} &= -1\\
a_{44} &= -\frac{k_{n3}}{k_{n2}}\exp(-ik_{n3}t_3)\\
a_{45} &= \frac{k_{n3}}{k_{n2}}\exp(ik_{n3}t_3)\\
a_{54} &= 1\\
a_{55} &= 1\\
a_{56} &= -1\\
a_{57} &= -1\\
a_{64} &= 1\\
a_{65} &= -1\\
a_{66} &= -\frac{k_{n4}}{k_{n3}}\\
a_{67} &= \frac{k_{n4}}{k_{n3}}\\
a_{76} &= \exp(-ik_{n4}t_4)\\
a_{77} &= \exp(ik_{n4}t_4)\\
a_{78} &= -1\\
a_{79} &= -1\\
a_{86} &= \frac{kn4}{k_{n5}}\exp(ik_{n4}t_4)\\
a_{87} &= -\frac{k_{n4}}{k_{n5}}\exp(-ik_{n4}t_4)\\
a_{88} &= -1\\
a_{89} &= 1\\
a_{98} &= \exp(ik_{n4}t_5)\\
a_{99} &= \exp(-ik_{n5}t_5)\\
a_{910} &= -1\\
a_{911} &= -1\\
a_{108} &= \frac{k_{n5}}{k_{n6}}\exp(ik_{n5}t_5)\\
a_{109} &= -\frac{k_{n5}}{k_{n6}}\exp(-ik_{n5}t_k)\\
a_{1010} &= -1\\
a_{1011} &= 1\\
a_{1110} &= \exp(ik_{n6}t_6)\\
a_{1111} &= \exp(-ik_{n6}t_6)\\
a_{1112} &= \sin(k_{n7}t_7)\\
a_{1210} &= i\frac{k_{n6}}{k_{n7}}\exp(ik_{n6}t_6)\\
a_{1211} &= -i\frac{k_{n6}}{k_{n7}}\exp(-ik_{n6}t_6)\\
a_{1212} &= -\cos(k_{n7}t_7)\\
b_{71} &= -T_n(t_4)\\
b_{81} &= i\frac{T_n'(t_4)}{k_{n5}}.
\end{aligned}
$$

The solution of (A-3) is obtained via the perturbation technique [24], which consists of assuming that all partial waves are driven by the fundamental component $n = 0$. Since for $n = 0$ the RHS of (A-3) is zero, all we have to do is calculate β_0 by solving $\det(\boldsymbol{Q}) = 0$. Once β_0 is calculated, β_n $(-\infty \le n \le \infty, n \neq 0)$ is obtained according to

$$\beta_n = \beta_0 + n\frac{2\pi}{\Lambda}, \qquad n = 0, \pm 1, \pm 2, \pm 3, \cdots, \tag{A-4}$$

where Λ is the grating period. The amplitudes A_{nj} and B_{nj} $(j = 1, 2, \cdots, 7)$ are now easily calculated through a simple matrix operation, i.e., $\boldsymbol{Q} \cdot \boldsymbol{X} = \boldsymbol{T}$ or $\boldsymbol{X} = \boldsymbol{Q}^{-1} \cdot \boldsymbol{T}$.

REFERENCES

[1] J. M. Hammer, R. A. Bartolini, A. Miller, and C. C. Neil, "Optical grating coupling between low-index film and waveguides," *Appl. Phys. Lett.*, vol. 28, no. 4, pp. 192–194, Feb. 15, 1976.

[2] N.-H. Sun, J. K. Butler, J.-P. Sih, G. A. Evans, and L. Pang, in *Proc. Conf. Lasers Electro-Opt.*, Anaheim, CA, June 2–7, 1996, pp. 217–218.

[3] D. L. Lee, *Electromagnetic Principles of Integrated Optics*. New York: Wiley, 1986.

[4] G. Griffel, M. Itzkovich, and A. Hardy, "Coupled mode formulation for directional couplers with longitudinal perturbation," *IEEE J. Quantum Electron.*, vol. 27, pp. 985–994, Apr. 1991.

[5] Y. Chen and A. Snyder, "Grating-assisted couplers," *Opt. Lett.*, vol. 16, no. 4, pp. 217–219, 15 Feb. 1991.

[6] J. P. Donnelly, H. A. Haus, and L. A. Molter, "Cross power and crosstalk in waveguide couplers," *J. Lightwave Technol.*, vol. 6, pp. 257–267, Feb. 1988.

[7] W.-P. Huang and H. Haus, "Power exchange in grating-assisted couplers," *J. Lightwave Technol.*, vol. 7, pp. 920–924, June 1989.

[8] W. Huang, B. E. Little, and S. K. Chaudhuri, "A new approach to grating-assisted couplers," *J. Lightwave Technol.*, vol. 9, pp. 721–727, June 1991.

[9] J. Hong and W. Huang, "Contra-directional coupling in grating-assisted guided-wave devices," *J. Lightwave Technol.*, vol. 10, pp. 875–881, July 1992.

[10] H. A. Haus, W. P. Huang, and N. A. Whitaker, "Coupled-mode theory of optical waveguides," *J. Lightwave Technol.*, vol. LT-5, pp. 16–23, Jan. 1987.

[11] H. A. Haus, W. P. Huang, and A. W. Snyder, "Coupled-mode formulations," *Opt. Lett.*, vol. 14, no. 21, pp. 1222–1224, Nov. 1, 1989.

[12] B. E. Little and H. A. Haus, "A variational coupled-mode theory for periodic waveguides," *IEEE J. Quantum Electron.*, vol. 31, pp. 985–994, Dec. 1995.

[13] W. Huang and J. Hong, "A transfer matrix approach based on local normal modes for coupled waveguides with periodic perturbations," *J. Lightwave Technol.*, vol. 10, pp. 1367–1375, Oct. 1992.

[14] M. N. Weiss and R. Srivastava, "Spectral characteristics of asymmetric directional couplers in graded index channel waveguides analyzed by coupled-mode and normal-mode techniques," *Appl. Opt.*, vol. 34, no. 6, pp. 1029–1040, Feb. 20, 1995.

[15] D. Marcuse, "Directional couplers made of nonidentical asymmetric slabs. Part II: Grating assisted couplers," *J. Lightwave Technol.*, vol. LT-5, pp. 268–273, Feb. 1987.

[16] ———, *Theory of Dielectric Optical Waveguides*, 2nd ed. New York: Academic, 1991.

[17] S. L. Chuang, "A coupled mode formulation by reciprocity and a variational principle," *J. Lightwave Technol.*, vol. LT-5, pp. 5–15, Jan. 1987.

[18] W. Zubrzycki, B. V. Borges, P. R. Herczfeld, S. H. Kravitz, J. C. Word, and R. F. Corless, "Design of an integrated optic Fabry–Perot optical modulator for microwave applications," in *Proc. 24th European Microwave Symp.*, vol. II, Cannes, France, Sept. 5–8, 1994, pp. 1459–1464.
[19] W. Zubrzycki, B. V. Borges, P. R. Herczfeld, S. H. Kravitz, G. R. Hadley, G. A. Vawter, R. F. Corless, R. E. Smith, J. R. Wendt, J. C. Word, and T. M. Bauer, "Integrated optic distributed Bragg reflector Fabry–Perot modulator for microwave applications," *Proc. Int. Microwave Symp.*, vol. 1, Orlando, FL, May 1995, pp. 259–262,.
[20] T.-D. Ni, D. Sturzebecher, M. Cummings, and B. Perlman, "Design, fabrication, and test of wide-angle low-loss Y-junction hybrid polymer couplers," *Appl. Phys. Lett.*, vol. 67, no. 12, pp. 1651–1652, Sept. 1995.
[21] K.-H. Schlereth and M. Tacke, "The complex propagation constant of multilayer waveguides: An algorithm for a personal computer," *IEEE J. Quantum Electron.*, vol. 26, pp. 627–630, Apr. 1990.
[22] W. H. Press, B. P. Flannery, S. A. Teukolsky, and W. T. Vetterling, *Numerical Recipes: The Art of Scientific Computing*. Cambridge, U.K.: Cambridge Univ. Press, 1986.
[23] G. A. Peterson, "Reflection, transmission, and scattering at an integral diode laser-waveguide interface," *SPIE Laser-Diode Technol. Applicat. II*, vol. 1219, pp. 435–443, 1990.
[24] W. Streifer, D. R. Scifres, and R. D. Burnham, "Analysis of grating-coupled radiation in GaAs:GaAlAs lasers and waveguides," *IEEE J. Quantum Electron.*, vol. QE-12, pp. 422–428, July 1976.
[25] E. Butkov, *Mathematical Physics* (Series in Advanced Physics). Reading, MA: Addison-Wesley, 1968.

B.-H. V. Borges was born in Governador Valadares, Minas Gerais, Brazil, in 1963. He received the B.Sc. degree in electrical engineering from the Universidade do Vale do Rio Doce (UNIVALE), Governador Valadares, Brazil, in 1987, the M.Sc. degree in electrical engineering from the University of São Paulo, São Carlos, Brazil, in 1992, and the Ph.D. degree from Drexel University, Philadelphia, PA, in 1997.

He is currently at the University of São Paulo, São Carlos, Brazil. His interests include modeling of linear and nonlinear optical waveguides, grating assisted devices, electro-optic modulators, fiber-optic sensors, and integrated optic sensors.

P. R. Herczfeld (S'66–M'67–SM'89–F'91) was born in Budapest, Hungary, in 1935. He received the B.Sc. degree in physics from Colorado State University, Fort Collins, in 1961, and the M.Sc. degree in physics and Ph.D. degree in electrical engineering from the University of Minnesota at Minneapolis, St. Paul, in 1963 and 1967, respectively.

Since 1967, he has been on the faculty of Drexel University, Philadelphia, PA, where he is both a Professor of electrical and computer engineering, and Director of the Center for Microwave–Lightwave Engineering. He has authored or co-authored over 300 papers in solid-state electronics, microwaves, photonics, solar energy, and biomedical engineering, and has served as Project Director for over 70 projects.

Dr. Herczfeld is a member of APS, SPIE, and ISEC, and is recipient of several research and publication awards, including the Microwave Prize in 1986 and 1987.